RSC Advances

ROYAL SOCIETY OF CHEMISTRY

www.rsc.org/advances

A new organic–silica based nanocomposite prepared for spectrophotometric determination of uranyl ions

A. M. El Nahrawy[a], O. A. Elhefnawy[b], A. A. Elabd[b,*]

[a] Department of Solid State Physics, National Research Centre (NRC)-33 El Bohouth st.,(former ElTahrir st.), Dokki, Giza, P.O.12622, Egypt

[b]Nuclear Safeguards and Physical protection Department, Nuclear and Radiological Regulatory Authority (NRRA), P.O. Box 7551, Cairo, Egypt

[*]Corresponding author:

a.a.elabd@gmail.com

Tel: +2 0122 5781529

Fax: +2 2274 02 38

Abstract

A new organic–silica based nanocomposite has been prepared for uranyl ions (UO_2^{2+}) determination based on the absorbance enhancement of Tartrazine incorporated copper sodium silicate nanocomposite (**T-CSS**). **T-CSS** has been characterized by Fourier Transforms Infrared Spectroscopy (FTIR), X-Ray Diffraction (XRD), Scanning Electron Microscopy/Energy Dispersive X-Ray Spectroscopy (SEM/EDX) and Transmission Electron Microscopy (TEM). The UO_2^{2+}/ **T-CSS** complex shows a maximum absorption at 252 nm with a molar absorptivity of 6.5 x 10^3 L mol^{-1} cm^{-1}. Beer's law has been applied in range of 2.0x10^{-5}–1.5x10^{-4} mol L^{-1}. For more accurate analysis, Ringbom optimum concentration range was 2.1x10^{-5}–1.3x10^{-4} mol L^{-1}. Sandell sensitivity, detection and quantification limits have been calculated. Also, **T-CSS** was applied on the determination of UO_2^{2+} in real samples. The results have been compared with Inductively Coupled Plasma Optical Emission Spectrometry (ICP-OES) data, very similar values were found by the two methods.

Keywords: *Composite material; Nanostructure; Chemical technique; Electron microscopy.*

1. Introduction

Uranium is generally found at low levels within all rock, soil and water samples, combined with other elements. The increase in nuclear power production predominantly based on uranium fuel cycle causes the release of uranium and other radionuclides into the waste of such industrial process. [1,2] Radiological impact and chemical toxicity of uranium depend on its chemical form and concentration.[3–5] Uranium is an element that naturally presents in various oxidation states (II- VI), but VI is the most stable oxidation state. Usually in nature, uranium is associated with oxygen, forming the uranyl ions (UO_2^{2+}).[6] Determination of UO_2^{2+} is usually required in the process waste solutions and also as an impurity in the product materials of other nuclear elements.[7,8] Hence, for reasons of safety, security and safeguards, uranium is an important fuel constituent that needs to determine its concentrations.

Spectrophotometric technique is widely used for determination of heavy metals due to their simplicity, rapidity, low costs and wide applications. The organic–inorganic nanocomposite materials are currently the objects of intensive research.[9-11] Carotenuto et al. prepared nanocomposite thin films for optical devices.[12] Shu et al. developed a

phosphorescence sensor for H_2O_2 based on TiO_2/SiO_2 composite.[13] Yan et al. prepared a selective dopamine biosensor based on AgCl-polyaniline core–shell nanocomposites.[14] Habibi and Askari prepared nanostructure zinc zirconate composite for Spectrophotometric studies of photo-induced degradation of tertrodirect light blue.[15] Chang and Tang prepared nanocomposite from glucose oxidase and magnetite nanoparticles immobilized on graphene oxide and applied to the determination of glucose in human serum samples.[16] Y. Sun and Y. Xia reported that the surface plasmon resonance of gold nanoshells exhibited a much more sensitive response toward environmental changes even when compared with solid colloids with a mean size much smaller than that of gold nanoshells. Such enhanced sensitivities should make gold nanoshells particularly useful as optical probes for chemical or biological binding events at solid−liquid interfaces.[17]

Recently, the development in silicate systems have been great interest in many application especially optoelectronic, sensors and biological due to their structures and compositions.[18-21] The textural properties for silica (SiO_2) prepared by sol gel process increases with the addition of different types of modifiers such as alkali and transition

elements. So the addition of (Na and Cu) into the silica matrix was induced the network disruption.[22-24] The sol gel sodium silicate consists of silanol groups that may condense to form siloxane bridges (Si-O-Si-), (Si-O-Na-) and (Si-O-Cu-). Therefore, the surface composition of sodium silicate gel is made of physically adsorbed water, chemically bound water and silicon dioxide.[25] Tartrazine is a synthetic industrial azo-dye, primarily used as a food dye and various types of medications.[26] Addition of Tartrazine to copper sodium silicate matrix is improving the feature of the silicate matrix by helping to open the silicate structure and increase solubility by forming a new non-bridging group between the dye and the semiconducting system.[22-24]

In this study, a new organic–silica based nanocomposite has been prepared for UO_2^{2+} determination based on the absorbance enhancement of Tartrazine incorporated copper sodium silicate nanocomposite (**T-CSS**). **T-CSS** has been characterized by Fourier Transforms Infrared Spectroscopy (FTIR), X-Ray Diffraction (XRD), Scanning Electron Microscopy/Energy Dispersive X-Ray Spectroscopy (SEM/EDX) and Transmission Electron Microscopy (TEM).**T-CSS** was shown fast response time, stability and low

detection limit. **T-CSS** was applied for determination of UO_2^{2+} in different real samples with satisfactory results.

2. Materials and methods

2.1. Materials

All chemicals were used without further purification throughout the experiments. Uranyl nitrate hexahydrate, $UO_2(NO_3)_2{\cdot}6H_2O$ was manufactured by Mallinckrodt Company. Tetraethoxysilane (TEOS) was purchased from Aldrich Company. All other reagents were purchased from Merk Company. The pH was adjusted by using 0.1 M of HCl / NaOH.

2.2. Instruments

All absorbance spectra were recorded with a UV – Vis Evolution 300, using quartz cells with 10 mm optical path length from Thermo Fisher Scientific Company, UK. Fourier Transforms Infrared Spectroscopy (FTIR), (Jasco FT/IR-6100 type A, USA) was used to investigate the structure of **T-CSS.** Structure and purity of **T-CSS** were investigated by X-Ray Diffraction (XRD) on a Bruker D8 Advance diffractometer. Surface morphology and

distribution of elements of **T-CSS** were investigated by Scanning Electron Microscopy (SEM), with an Energy Dispersive X-Ray **(**EDX) detector (JEOL, 6510 LA, Japan). Transmission Electron Microscope (TEM) image was obtained by (JEOL JEM-2100, Japan). Inductively Coupled Plasma Optical Emission Spectrometry (ICP-OES) was used for determination of uranium concentrations as a reference measured by (iCAP 6500 ICP-OES, Thermo Fisher Scientific, UK), with ITEVA operating software. To ensure the accuracy of measurement, U concentrations calculated from emission intensities measured at two wavelengths as follows: U(385.958{87}) and U(409.014{82}) confirmed that each dataset is consistent in itself. In addition, certified reference material was analyzed in regular intervals during the measurement sequence. While no perfectly matrix-matched reference materials are available. Measurement of pH was performed using a Jenway pH meter. All measurements were performed at room temperature. The experimental work was carried out at safeguards analytical laboratory (ETZ-, KMP-I) at the Nuclear and Radiological Regulatory Authority (NRRA).

2.3. Preparation of Tartrazine / copper sodium silicate nanocomposite (T-CSS)

The synthesis of silica sol using TEOS, ethanol, deionized water and HCL, with the ratio (1.0: 6.0: 5.0: 0.75) was stirred for 1 h. The two modifiers, Sodium nitrate and copper nitrate were dissolved in deionized water and then added into the silica sol under continuous stirring for 1h. 0.3 mg of Tartrazine was dissolved in deionized water and added to previous sol under continuous stirring for another 1h. The resultant homogeneous solution of Tartrazine /copper sodium silicate **(T-CSS)** was filled in a glass vials and aged three weeks at room temperature and then in an oven at 300 ^{o}C for 5 h. **T-CSS** was characterized by IR, XRD, SEM/EDX and TEM.

2.4. Procedure

A suitable aliquot containing between 4.0 and 45.0 ug of UO_2^{2+}, was mixed with 1.0 mL of 1.0×10^{-3} mol L^{-1} **T-CSS** and diluted to 10 mL ethanol at pH 5.5. The content of each flask was shaking well and the absorbance was measured at 252 nm against the reagent blank which prepared similarly as the previous solution but without UO_2^{2+}. The concentration of

UO_2^{2+} was calculated either from a calibration curve or a regression equation.

2.5. Determination of stoichiometry

The stoichiometric determination of UO_2^{2+}/**T-CSS** complex was conducted using a UV–vis spectrometry. Job's method was applied to establish the components ratio of the complexes. Different volumes (0, 0.2, 0.4, 0.6, 0.8, 1.0, 1.2, 1.4, 1.6, 1.8, 2.0 mL) of 1.0×10^{-3} mol L^{-1} UO_2^{2+} was mixed with different volumes (2.0, 1.8, 1.6, 1.4, 1.2, 1.0, 0.8, 0.6, 0.4, 0.2, 0 mL) of 1.0×10^{-3} mol L^{-1} **T-CSS** and diluted to 10 mL ethanol. The absorbance was recorded at λ_{max} = 252 nm and plotted against the mole fraction of UO_2^{2+}.

3. Results and discussion

3.1. Characterizations

3.1.1. Fourier Transform Infrared Spectroscopy (FTIR)

Figure 1 shows the FTIR spectra of samples (a): Copper Sodium Silicate (**CSS)** and (b): **T-CSS** nanocomposite. **CSS** has several absorption bands can be observed at 3640, 3463, 1663, 1060, 755, 482 and 445 cm^{-1}. The bands at 3640, 3463 cm^{-1} are assigned to the –OH stretching vibration, and the band at 1663 cm^{-1} is attributed to the –OH bending vibrations or to the C-H groups bonded with Tartrazine.[27, 28] The bands at 1060, 755, cm^{-1} are

assigned to the stretching and the bending vibration modes of (Si–O–Si), (Si–O–Cu), (Na–O–Si) (Si-O).[29, 30] While the bands at 482 and 445 cm^{-1} are assigned to a well-formed crystalline phase of silica in tetrahedral coordination with respect to oxygen [SiO_4], or may be assigned to normal stretching and bending vibration modes of (Cu-O).[31-33] The **T-CSS** peaks appeared in the same regions of **CSS** with slight shift in spectrum at 3420, 1600, 1167, 798, 462, and 420 cm^{-1}, which believed that **T-CSS** is a composite of copper sodium silicate (**CSS**). The broad band in 3420 cm^{-1} combines the bands 3640 and 3463 cm^{-1} in **CSS** and the broad band 1167 cm^{-1} are may be assigned to the lower temperature 300 ^{o}C, which doesn't give a high degree of crystallinity of the prepared **T-CSS** at 300 ^{o}C**.** The slight shift of the **T-CSS** bands from **CSS** bands may be due to the formation of a type of interaction between Tartrazine and **CSS**.

3.1.2. X-Ray Diffraction (XRD)

The XRD pattern of **T-CSS** nanocomposite compared with XRD card of a crystalline phase of copper sodium silicate ($CuNa_2Si_4O_{10}$) as shown in Fig.2. There is no obvious difference between **T-CSS** pattern and the card. **T-CSS** is matching well with the crystalline phase of copper sodium silicate which confirms that **T-CSS** is a monoclinic copper sodium silicate according

to (JCPDS: 70-0352). The broad band between the 2θ angles of 18° and 30° in the pattern referrers to the amorphous nature of the **T-CSS** at 300 ^{o}C. The XRD pattern proves that the prepared **T-CSS** is an amorphous phase of copper sodium silicate ($CuNa_2Si_3O_8$).

3.1.3. Scanning Electron Microscopy and Energy Dispersive X-Ray Spectroscopy (SEM/EDX)

Figures 3 (a, b) shows the SEM image of **T-CSS** nanocomposite at lower and higher magnification, respectively. The surface morphology of the SEM images showed irregular shapes of the **T-CSS** nanocomposite as shown in Fig. 3(a). Fig. 3(b) shows the magnifying SEM image of **T-CSS** nanocomposite which seems like a thin layers stacked on top of each other therefore, **T-CSS** nanocomposite composed of particles with a considerable tendency to agglomerate. Figure 4 shows EDX spectrum of **T-CSS** nanocomposite, which indicates that **T-CSS** nanocomposite contains C, O, Si, Na and Cu.

3.1.4. Transmission Electron Microscopy (TEM)

Figure 5 shows the TEM image of **T-CSS**. It looks like a spherical shape accumulates to each other with a nanoparticle size around = 17-30 nm. The

nanoparticle size is depending on different factors, including the stirring rate, the reaction temperature and the addition rate of the modifiers into the sol.

3.2. Absorption spectra

The absorption spectra of **T-CSS** and UO_2^{2+}/**T-CSS** complex in ethanol solution are shown in Fig. 6. Figure 6 shows that, no absorption band was observed at 252 nm for **T-CSS**. However, upon addition of different concentrations of UO_2^{2+} to **T-CSS**, the absorption band formed at 252 nm and increased with UO_2^{2+} concentrations increased, that attributed to the formation of UO_2^{2+}/**T-CSS** complex. The absorption band at UV range (252 nm) refers to the complex formation between UO_2^{2+} and copper sodium silicate matrix and there is no bands appeared in visible range which indicated that there is no reaction between UO_2^{2+} and Tartarzine. Although the Tartrazine doesn't share in the complex formation, the Addition of Tartrazine to copper sodium silicate matrix is improving the feature of the silicate matrix by helping to open the silicate structure and increase solubility by forming a new non-bridging group between the dye and the semiconducting system.[22-24] The band at 252 nm may occur due to the intramolecular charge transfer (ICT) transitions within the whole structure.

When the UO_2^{2+} contact with **T-CSS**, the intermolecular proton transfer take places between Si-O- and UO_2^{2+}. The modulation in the electron donating abilities of Si-O- in the presence and absence of UO_2^{2+} directly influences ICT transitions within the whole structure. In the absence of UO_2^{2+}, ICT is inefficient while in the presence of UO_2^{2+}, ICT is facilitated by proton transfer from Si-O- to UO_2^{2+}. Thus, it is proposed that the spectral changes in Fig. 6 is due to the deprotonation of the Si-O- protons, which enhanced the charge transfer interactions between electron rich and electron deficient moieties forming a new band at 252 nm. Therefore, based on the literature background and our experimental findings, the schematic representation of the complexation process of UO_2^{2+}/**T-CSS** is shown in Fig. 7. Under optimized conditions, [The conditions are UO_2^{2+} content (4.0 - 45.0 ug); **T-CSS** (1.0 mL of 1.0 × 10^{-3} mol L^{-1})**;** pH 5.5 and λ_{max} = 252 nm]the absorbance intensity of UO_2^{2+}/**T-CSS** was increased linearity with increased the concentration of UO_2^{2+}, which demonstrates that the chelating reaction between **T-CSS** and UO_2^{2+} can be used as spectrophotometric measured for UO_2^{2+} determination. In this study the absorbance intensity at 252 nm was selected for UO_2^{2+} determination.

3.3. Stoichiometry of the complexes

The stoichiometry of UO_2^{2+}/**T-CSS** was established by Job's method of continuous variation at 252 nm. This is due to the interaction of UO_2^{2+} with **T-CSS** at λ_{max}= 252 nm. The plot of absorbance versus mole fraction of UO_2^{2+} had revealed that the formation of the complex between UO_2^{2+} and **T-CSS** is 1:1 molar ratios at pH 5.5. (Fig.6 (inset)). It is expected that Na^+ atoms are replaced by UO_2^{2+}. The reason of that may be due to that the atomic and covalent radius of Na^+ is higher than that of Cu^{2+}. Consequently, ionization energy in case of Na^+ will be lower than that of Cu^{2+} and leads to lower energy per mole required to remove electrons from charged ions. This may explain that Na^+ atoms are replaced by UO_2^{2+} compared with Cu^{2+}.

3.4. Optimization

The effect of pH on the absorbance of the UO_2^{2+}/**T-CSS** complex at 252 nm in ethanol was studied against the reagent blank. Maximum absorbance was obtained at pH 5.5. At pH values more than 5.5, the response decreases. This could be due to the hydrolysis of the UO_2^{2+} in aqueous solutions, which results in the formation of different insoluble hydroxide forms of UO_2^{2+}.[5] Thus, it was not possible to examine pH effects

in alkaline solutions, as UO_2^{2+} precipitated in these media. The decrease in the response of the present sensor at low pH could be due to the competition of hydrogen ions and UO_2^{2+} for T-CSS.

The concentration of **T-CSS** was optimized by performing a series of experiments. The influence of the volume in the range of (0.1–2.0) mL of 1.0×10^{-3} mol L^{-1} **T-CSS** was examined at constant UO_2^{2+} concentration (1.0×10^{-4} mol L^{-1}). The maximum absorbance was attained with 1.0 mL of 1.0×10^{-3} mol L^{-1} **T-CSS**; above 1.0 mL, the absorbance remained unchanged. Therefore, 1.0 mL of 1.0×10^{-3} mol L^{-1} **T-CSS** was used in all further measurements.

Ethanol plays an important role in the solubility of **T-CSS** as well as UO_2^{2+}/ **T-CSS** complex, while they showed poor solubility in aqueous phase due to the presence of –OH groups through van-der-Waals force and hydrogen bond with water molecules. Thus, ethanol acted as a modifier phase. Hence in the presences of ethanol the absorbance intensity of UO_2^{2+}/ **T-CSS** complex was increased. So, addition of ethanol is necessary to avoid the phase separation by increasing the solubility of UO_2^{2+}/ **T-CSS** complex. Ethanol concentration was fixed at 5wt.% in the sample solutions.[34]

The time stability of UO_2^{2+}/ **T-CSS** complex was monitored as a function of time, which extended up to several hours. It was observed that the absorbance intensity of UO_2^{2+}/ **T-CSS** complex was stable up to >24 h.

3.5. Method validation

The proposed measured was validated according to ICH guidelines.[35]

3.5.1. Linearity and range

Under optimized conditions the absorbance of the complex was obeyed Beer's law in UO_2^{2+} concentration range of $2.0x10^{-5}$–$1.5x10^{-4}$ mol L^{-1} (Fig. 8). Regression analysis had been carried out with correlation coefficient (R^2, 0.997). The good linearity of the calibration graphs and negligible scatter of the experimental points are clearly evident by the value of R^2 and the standard deviation around the slopes and intercepts. For more accurate results, Ringbom optimum concentration range was determined by plotting log [UO_2^{2+}] against percent transmittance and the linear portion of the Z-shaped curve give the accurate range of analysis (Table 1). The molar absorptivities and Sandell sensitivities values of UO_2^{2+} were 6.5 x 10^3 L mol^{-1} cm^{-1} and 36.8 ng cm^{-2}, respectively. The limit of detection (LOD) is defined as the lowest amount of analyte in a sample which could be detected but not necessarily to be quantified as an exact

value. The limit of quantification (LOQ) is defined as the lowest amount of analyte in a sample which can be quantitatively determined with suitable precision and accuracy. The LOD and LOQ were calculated according to ICH guidelines[35] using the formulae: LOD= 3.3S/b and LOQ= 10S/b mol L^{-1} (where S is the standard deviation of blank absorbance value and b is the slope of the calibration plot) are indicated in Table 1.

3.5.2. Accuracy and precision

Accuracy was checked by standard addition method. Accuracy evaluated as percentage relative error (RE %) between the measured mean concentrations and the taken concentrations of UO_2^{2+}. RE {RE % = [(concentration found−known concentration) × 100/known concentration]} was calculated at each concentration. The range of RE % value was 0.84 – 1.66 % demonstrates the high accuracy of the proposed measured.

To compute the precision, the assays were repeated three times within the day to determine the repeatability (intra-day precision) and three times on different days to determine the intermediate precision (inter-day precision) of the method. The range of percentage relative standard deviation error (RSD %) values were 0.85 – 1.78 % (intra-day) and 0.96 – 1.48 % (inter-day) indicating high precision of the method.

3.5.3. Robustness and ruggedness

The robustness of the method was evaluated by making small incremental changes in the concentration of **T-CSS** and pH. The effect of the changes was studied on the absorbance intensity of UO_2^{2+}/ **T-CSS**. The changes had negligible influence on the results as revealed by small intermediate precision values expressed as RSD %. The results of this study are indicated in Table 2. The range of RSD % values were 1.14 – 2.62 % (**T-CSS** concentration) and 0.96 – 1.70 % (pH) indicating high precision of the method.

Method ruggedness was expressed as the RSD % of the same procedure applied by three different analysts. The results of this study are listed in Table 2. The inter-analysts RSD % was in a range of 1.86 – 3.23 % for the same UO_2^{2+} concentrations which suggested that, the developed method was rugged.

3.5.4. Selectivity

To study the selectivity of the proposed measured by **T-CSS** for spectrophotometric determination of UO_2^{2+}, the interference studies were carried out prior to the application of the proposed measured for the

determination of UO_2^{2+} in spiked aqueous solutions. The influences of several metal ions possibly existing in the real samples on the determination of UO_2^{2+} were examined by introducing them into the solutions containing 5.0 X 10^{-5} mol L^{-1} of UO_2^{2+} and treating as described in the procedure. The tolerance limit was fixed as the maximum amount of an ion causing an error no greater than 5% in absorbance intensity of the consequent solution. Figure 9 shows the tolerance limit for several metal ions. The results were indicated that, several metal ions do not interfere even at high concentrations. In addition to UO_2^{2+}, **T-CSS** also produces a response to some other metal ions as Al^{3+}, Fe^{3+} and Th^{4+} while the effects of most other foreign ions were low. It was reported in the literature that, some observed interfering effects were considerably diminished in the presence of 1,2-cyclohexylene dinitrilotetraacetic acid (CyDTA) as a proper masking agent.[36] So, the **T-CSS** has a good selectivity for spectrophotometric determination of UO_2^{2+} in aqueous solutions.

3.5.5. Application

In order to evaluate the performance of **T-CSS**, the UO_2^{2+} was applied to analysis in real samples. The real samples used in this work are sampled

from R&D lab. Most of them possess low concentrations of dissolved organic matters and the disadvantage of high transition metal ions level. The contents of UO_2^{2+} in aqueous real samples and RSD % are listed in Table 3. For further investigate of the performance of **T-CSS**, the results were compared with ICP-OES technique as a reference measured. As an indicated in Table 3, mean values were obtained with Student's t- and F-tests at 95% confidence limits. The results show comparable accuracy (t-test) and precision (F-value), since the calculated values are less than the theoretical data. It was observed that the results are very close to the measured values using ICP-OES technique. So the proposed measured can be helpful for UO_2^{2+} determination. The main advantages of the proposed measured over ICP OES technique are its simplicity, acceptable accuracy and lower cost.

4. Conclusions

A new **T-CSS** nanocomposite was prepared and characterized by different techniques. **T-CSS** was used for spectrophotometric determination of UO_2^{2+}, also various factors on the absorbance of UO_2^{2+}/ **T-CSS** were studied. The proposed measured has been applied for spectrophotometric determination of UO_2^{2+} in different real samples and the results were

statistically compared with those obtained by ICP-OES measured which show that, the Student's *t*- and *F*-values at 95% confidence level are less than the theoretical values. This confirms that there is no significant difference between the performance of a new **T-CSS** and ICP-OES measured. The proposed measured can be used to determine 4.0 – 45.0 ug of UO_2^{2+}, with high accuracy and precision.

References

1 A.A. Elabd, W.I. Zidan, M.M. Abo-Aly, E. Bakier and M.S. Attia, *Journal of Environmental Radioactivity*, 2014, 134, 99-108.

2 E.S. Craft, A.W. Abu-Qare, M.M. Flaherty, M.C. Garofolo, H.L. Rincavage, M.B. Abou-Donia and J. Toxicol. *Environ. Health B Crit. Rev.,* 2004, 7, 297.

3 S.J. Markich, *Sci. World J.,* 2002, 2, 707.

4 R. Hindin, D. Brugge and B. Panikkar, *Environ. Health,* 2005, 4, 17.

5 A.A. Elabd and M.S. Attia, *Journal of Luminescence,* 2015, 165,179–184.

6 *Uranium in drinking-water background document for development of WHO Guidelines for drinking-water Quality* (2005).

7 A.A. Elabd and M.S. Attia, *Journal of Luminescence,* 2016, 169,313–318.

8 A.A. Elabd and O.A. Elhefnawy, *Journal of Fluorescence,* DOI 10.1007/s10895-015-1709-8.

9 V. Ganesan and A. Walcarius, *J. Solid State Electrochem,* 2004, 20, 3632.

10 A.A. Khan and M.M. Alam, *Anal Chim Acta,* 2004, 504, 253.

11 L. Cui, R. Wang, X. Ji, M. Hu, B. Wang and J. Liu, *Materials Chemistry and Physics,* 2014, 148, 87-95.

12 G. Carotenuto , Y. Her and E. Matijević, *Ind. Eng. Chem. Res.*, 1996, 35, 2929–2932.

13 X. Shu, Y. Chen , H. Yuan, S. Gao and D. Xiao, *Anal. Chem.*, 2007, 79, 3695–3702.

14 W. Yan, X. Feng, X. Chen, X. Li and J. Zhu, *Bioelectrochemistry,* 2008, 72, 21-27.

15 M. H. Habibi and E. Askari, *Journal of Industrial and Engineering Chemistry,* 2013, 19, 1400-1405.

16 Q. Chang and H. Tang, *Microchim Acta*, 2014, 181, 527–534.

17 Y. Sun and Y. Xia, *Anal. Chem.*, 2002, 74, 5297–5305.

18 J. L. Gurav, A. V. Rao, A. P. Rao, D.Y. Nadargi and S.D. Bhagat, *Journal of Alloys and Compounds,* 2009, 476, 397–402.

19 F. Enrichi, R. Ricco`, A. Meneghello, R. Pierobon, E. Cretaio, F. Marinello, P. Schiavuta, A. Parma, P. Riello and A. Benedetti, *Opt Mater,* 2010, 32, 1652–1658.

20 D.Y. Shin, G. Cao and K.N. Kim, *Current Applied Physics,* 2011, 11, S309-S312.

21 A. Pandikumar and R. Ramaraj, *Journal of Hazardous Materials,* 2012, 203– 204, 244– 250.

22 I. Wacawska and M. Szumera, *J. Therm. Anal. Cal.,* 2006, 84, 185.

23 S. Sen and R.E. Youngman, *J. Non-Cryst. Solids,* 2003, 331, 100.

24 H. Aguiar, J. Serra, P. González and B. León, *Journal of Non-Crystalline Solids,* 2009, 355, 475–480.

25 Q. Lin, H. Peng, S. Zhong and J. Xiang, *Journal of Hazardous Materials,* 2015, 285, 199–206.

26 Food Standards Australia New Zealand. *Food Additives- Numerical List,* 2009.

27 X.H. Yang, W.L. Zhu and L.G. Li, *Ceram_Silika´ ty,* 2007, 51, 52–56.

28 O.A. Elhefnawy, W.I. Zidan, M.M. Abo-Aly, E.M. Bakier and G.A. Elsayed, *Journal of Radioanalytical and Nuclear Chemistry*, 2014, 299, 1821-1833.

29 R. Gaggiano, I.D. Graeve, J.M.C. Mol, K. Verbeken, L.A.I. Kestensc, and H. Terryna, *Surf. Interface Anal.,* 2013, 45, 1098–1104.

30 Y.S. Li, J.S. Church, A.L. Woodhead and F. Moussa, *Spectrochimica Acta Part A,* 2010, 76, 484–489.

31 T.E. Milja, K.P. Prathish and T.P. Rao, *Journal of Hazardous Materials,* 2011, 188, 384–390.

32 E.F. Medvedev and A.S. Komarevskaya, *Glass and Ceramics,* 2007, 64, 1-2.

33 M.A. Dar, Y.S. Kim, W.B. Kim, J.M. Sohn and H.S. Shin , *Applied Surface Science*, 2008, 254, 7477–7481

34 S. Ansari, A.R. Moghadassi and S.M. Hosseini, *Desalination,* 2015, 357, 189–196.

35 International Conference on Hormonisation of Technical Requirements for Registration of Pharmaceuticals for Human Use, ICH Harmonised Tripartite Guideline, Validation of Analytical Procedures: *Text and Methodology Q2(R1), Complementary Gui deline on Methodology dated 06 November 1996, incorporated in November 2005, London*.

36 K. Cheng, *Anal. Chem.,* 1958, 30, 1027–1030.

Figure captions

Fig. 1 FTIR spectra of samples (a) **CSS**, and (b) **T-CSS** nanocomposite.

Fig. 2 X-ray diffraction pattern of **T-CSS** nanocomposite and JCPDS card no. (JCPDS: 70-0352).

Fig. 3 SEM image of **T-CSS** nanocomposite (a) at low magnification 5,000 X and (b) at high magnification 20,000 X.

Fig. 4 EDX spectrum of **T-CSS** nanocomposite.

Fig. 5 TEM images of **T-CSS** nanocomposite.

Fig. 6 Absorption spectrum of T-CSS against a reagent blank in the presence of different concentrations of UO_2^{2+} at pH= 5.5. (Inset: Job's plot showing 1:1 stoichiometry).

Fig. 7 Schematic representation of the complexation process for **T-CSS** with UO_2^{2+}.

Fig. 8 Linear relation between UO_2^{2+} concentrations and absorbance of **T-CSS** at 252 nm and pH= 5.5 (Beer's low plot).

Fig. 9 Tolerance limit of different metal ions for determination of 5.0×10^{-5} mol L^{-1} UO_2^{2+}.

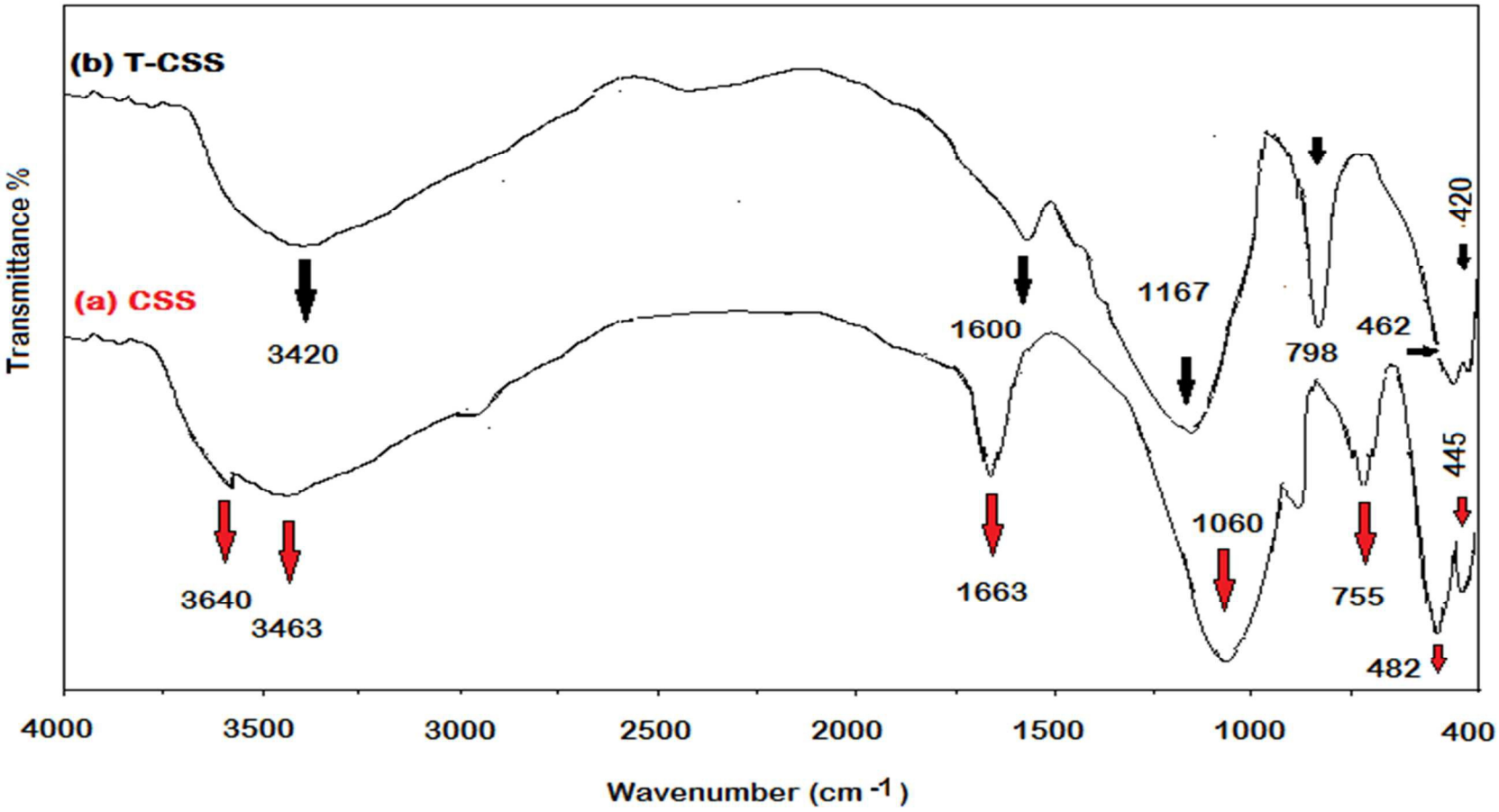

Fig.1.

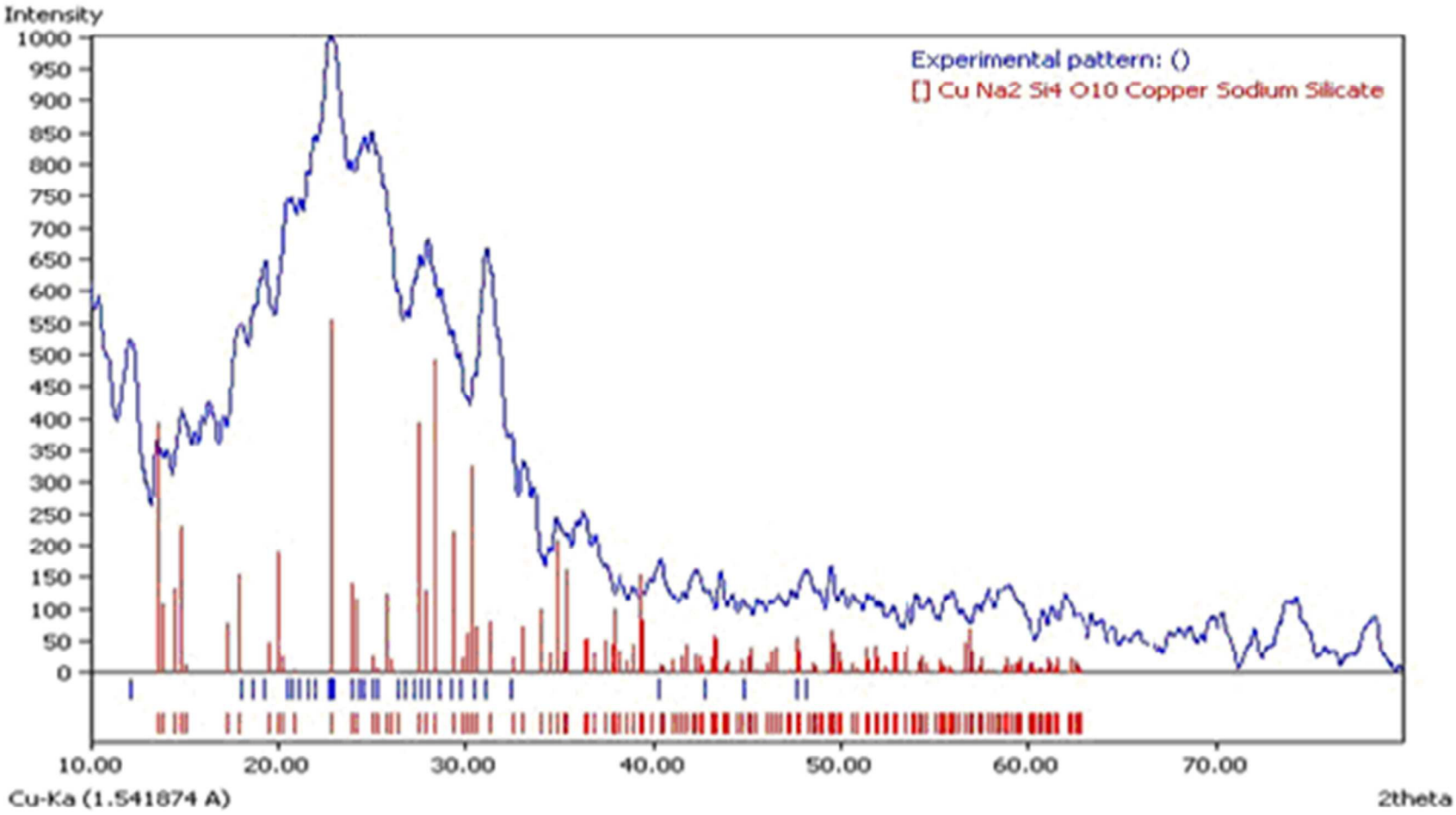

Fig.2.

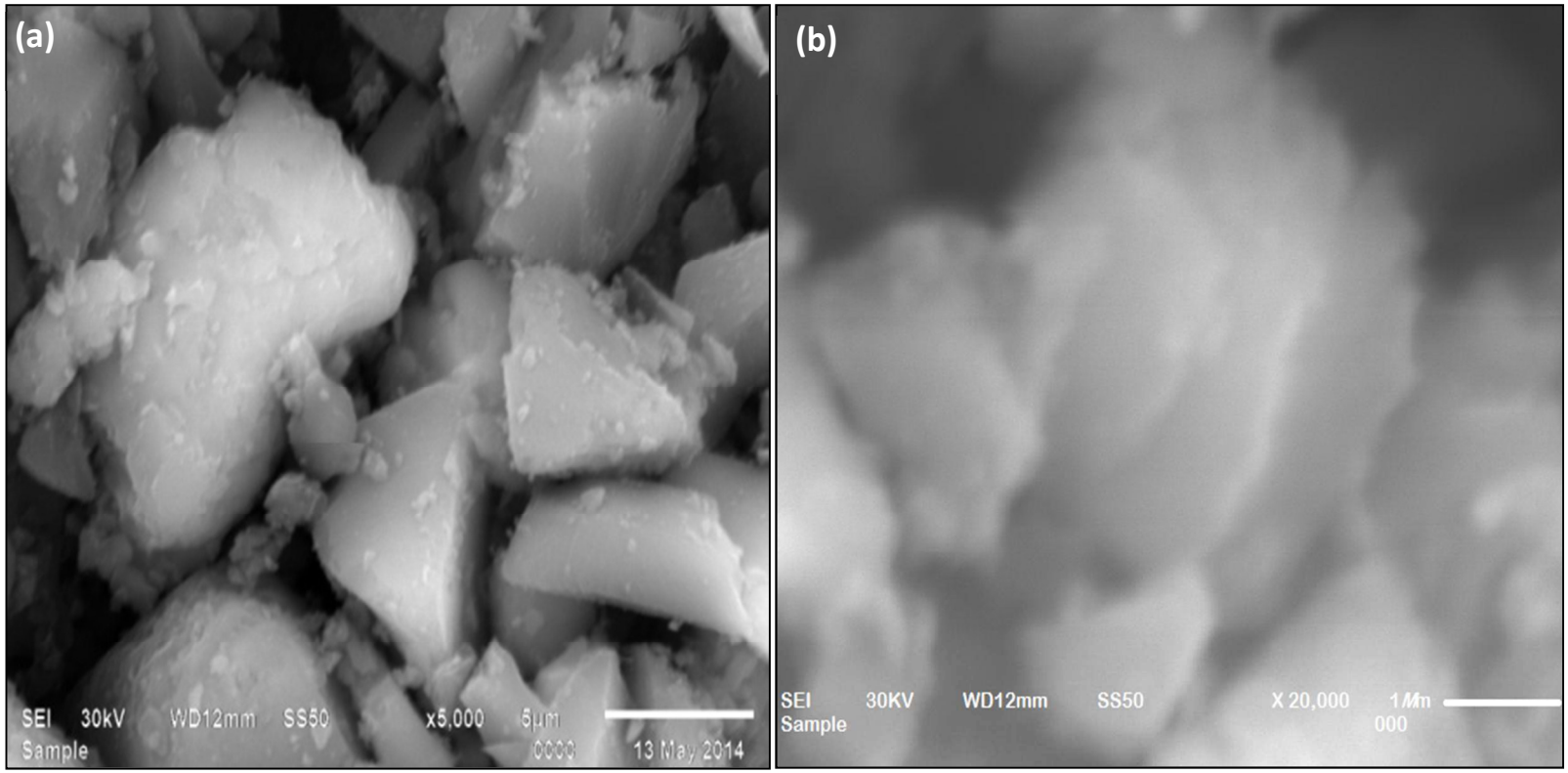

Fig. 3.

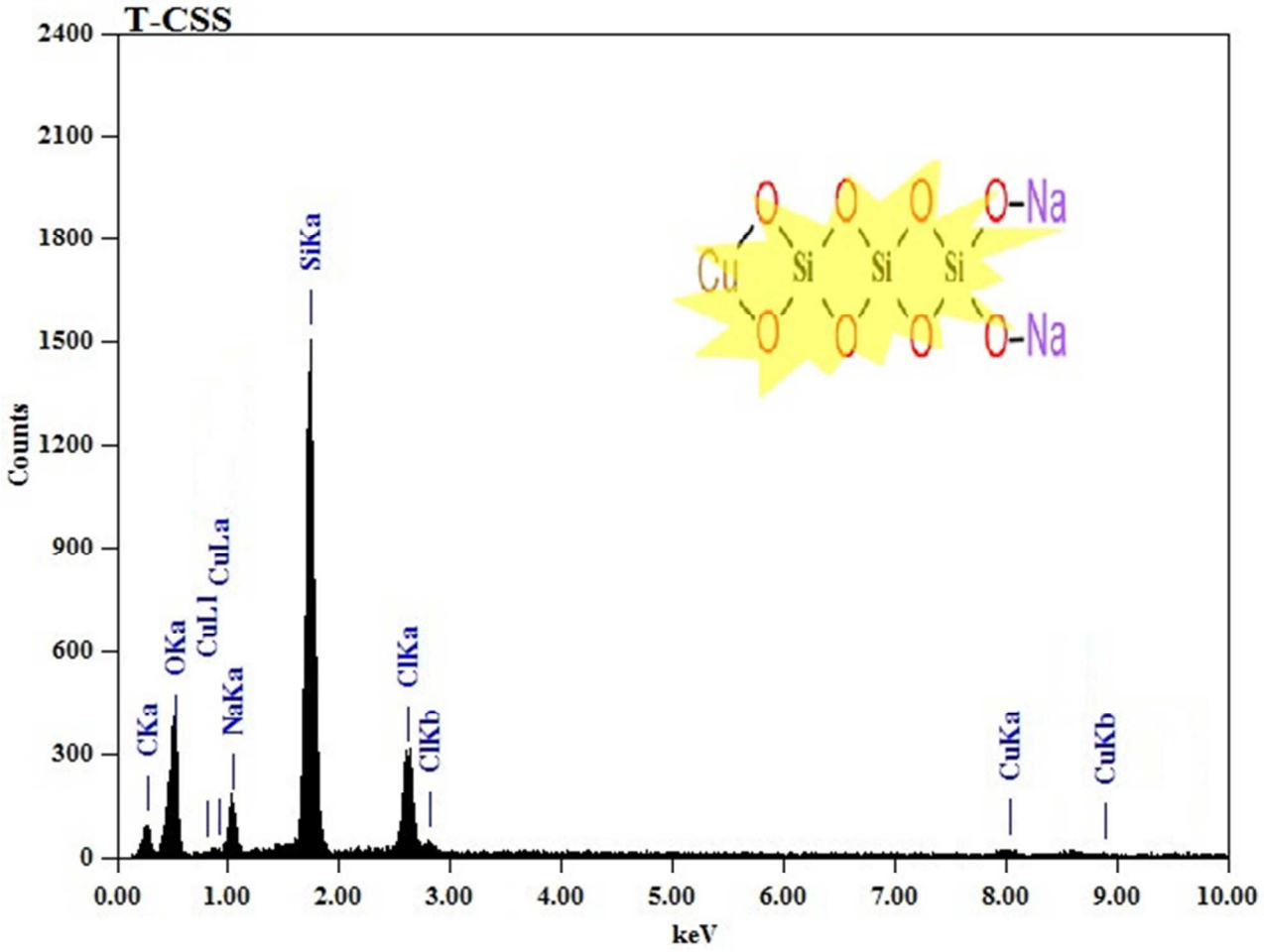

Fig. 4.

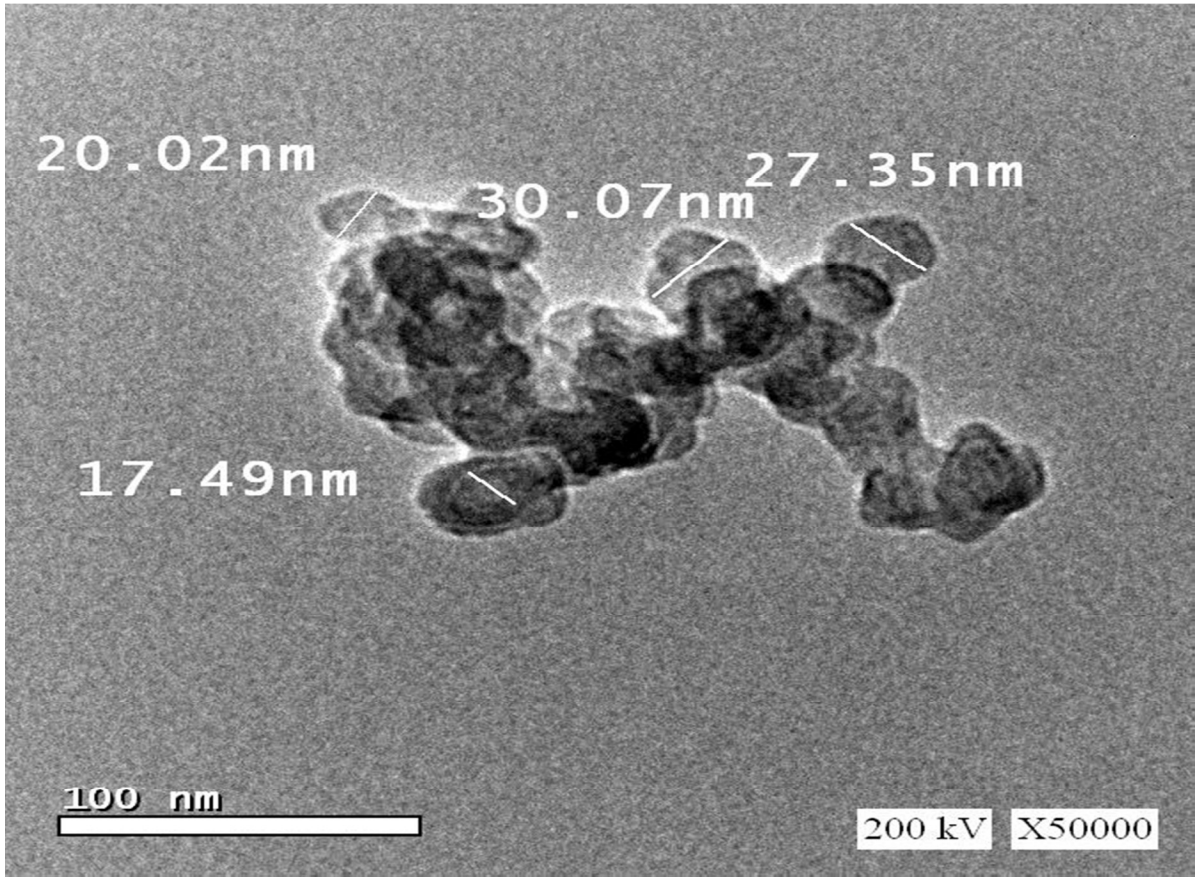

Fig. 5.

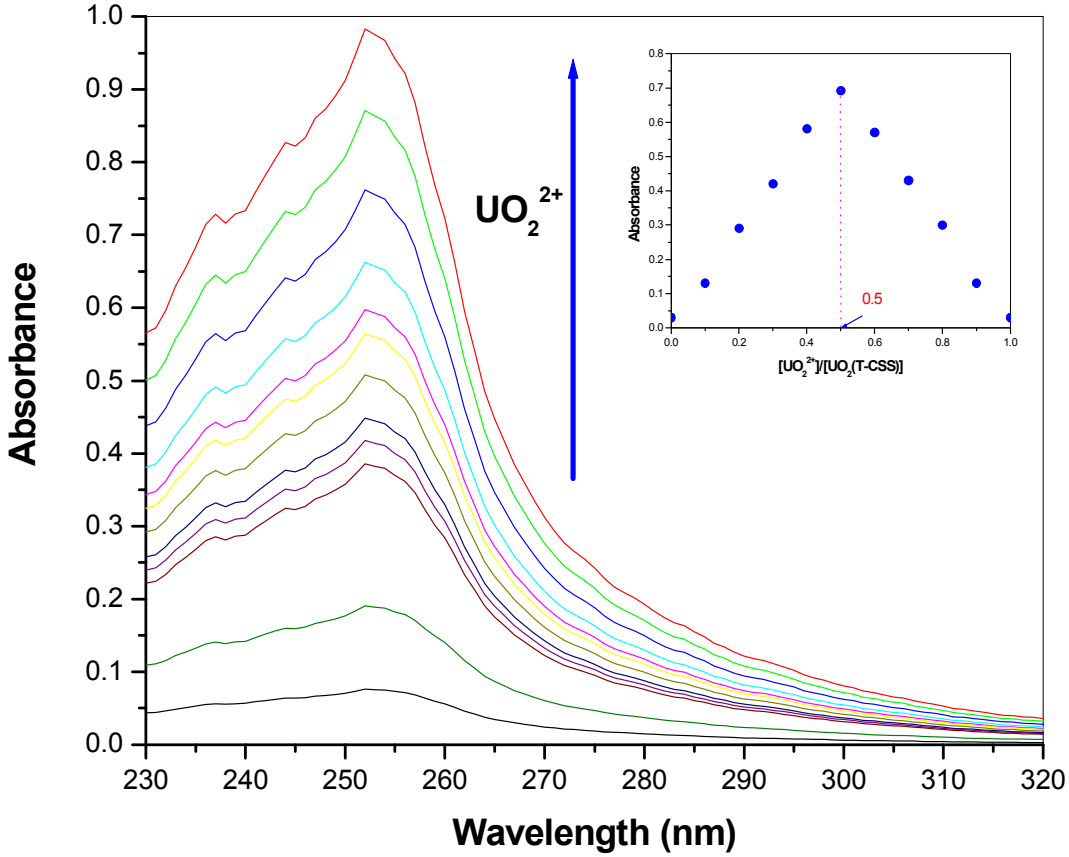

Fig. 6.

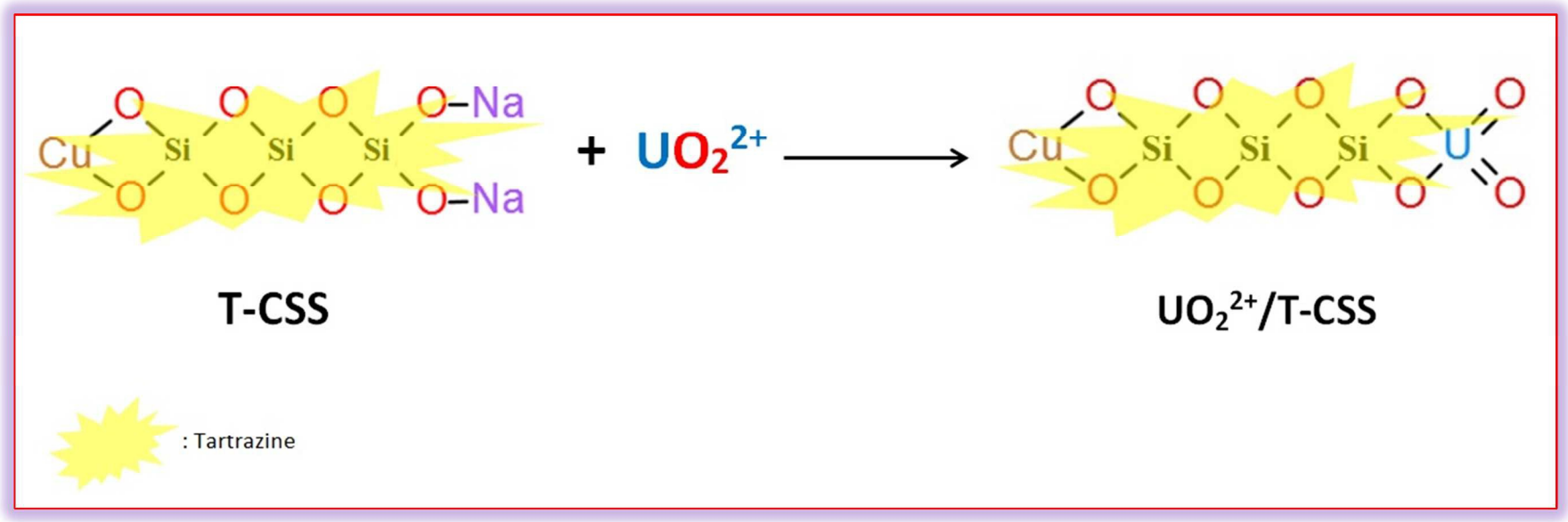

Fig. 7.

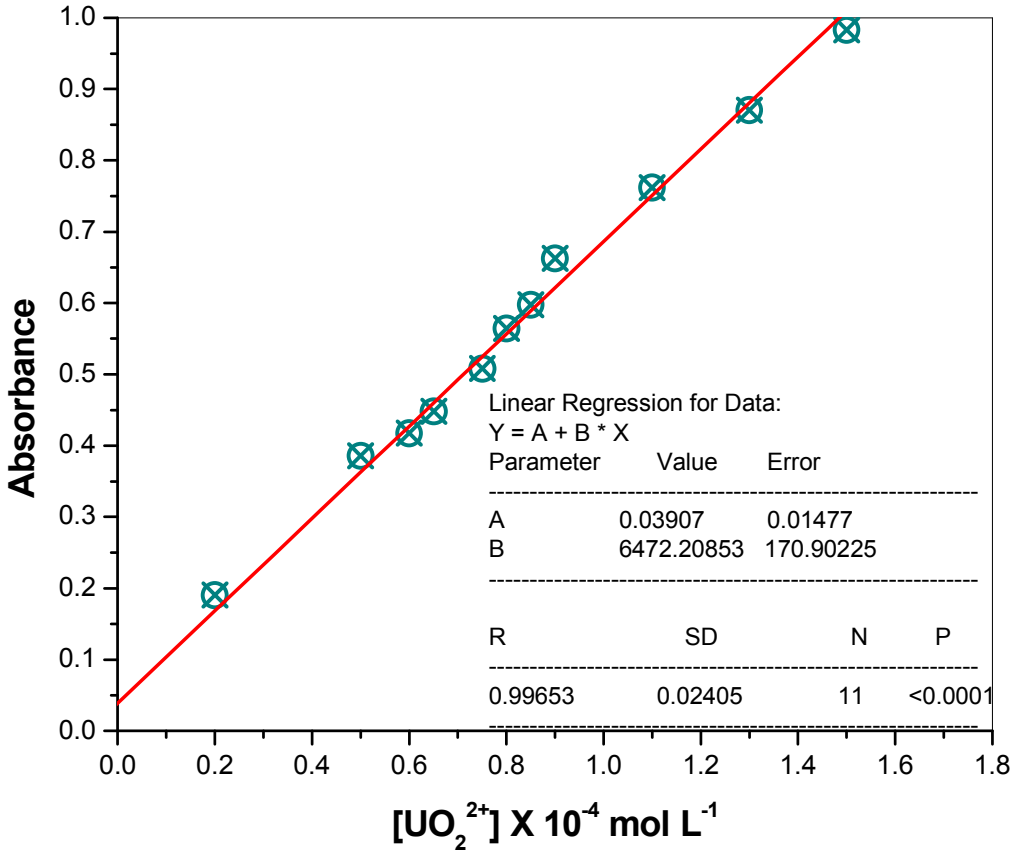

Fig. 8.

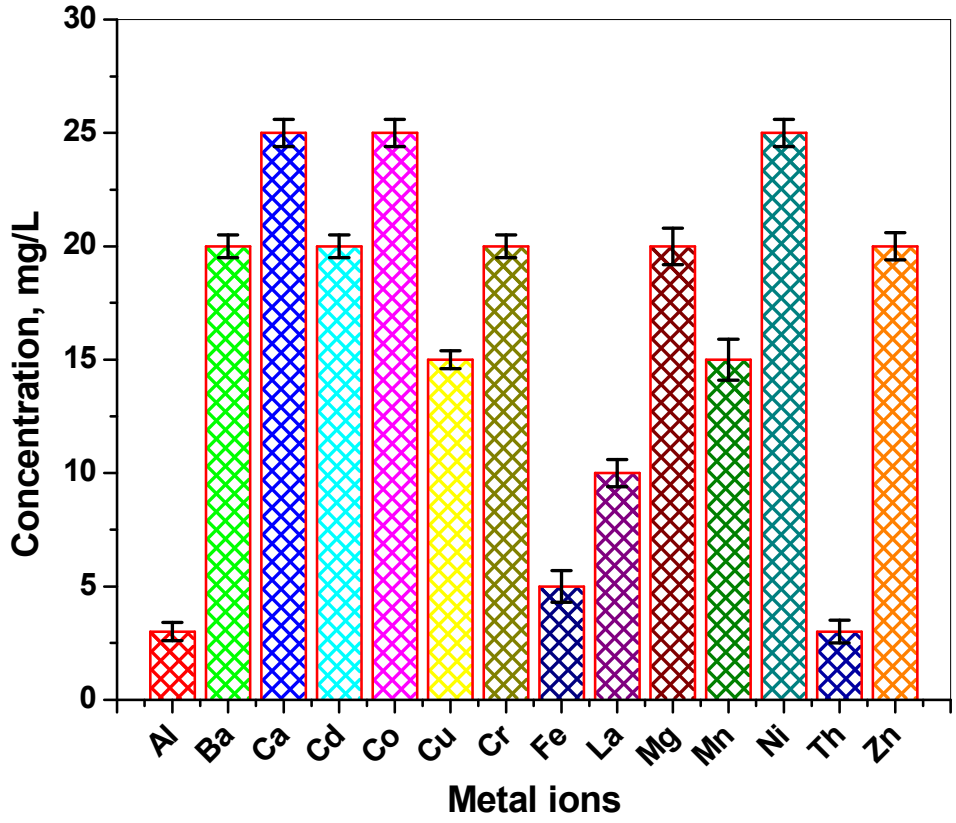

Fig. 9.

Table 1
Analytical characteristics of UO_2^{2+} with **T-CSS**.

Parameter	**Value**
Wavelength, (nm)	252
Molar absorptivity, (L mol^{-1} cm^{-1})	6.5×10^3
Linear range, (mol L^{-1})	$2.0 \times 10^{-5} – 1.5 \times 10^{-4}$
Ringbom, (mol L^{-1})	$2.1 \times 10^{-5} – 1.3 \times 10^{-4}$
Sandell's sensitivity, (ng cm^{-2})	36.8
Limit of detection, (mol L^{-1})	1.2×10^{-5}
Limit of quantification, (mol L^{-1})	3.7×10^{-5}
Standard deviation	0.024
Variance, (Sa^2)	5.8×10^{-4}
Correlation coefficient (R^2)	0.997

Table 2

Method robustness and ruggedness expressed as intermediate precision (%RSD).

Sample	UO_2^{2+} Spiked [a]	Robustness (n = 3)		Ruggedness (n = 3)
		Chemosensor conc. [b] (%RSD)[c]	pH [b] (%RSD)[c]	Inter-analysts, (%RSD)[c]
Tap water	5	1.94	1.48	2.48
	10	1.78	1.70	2.50
Well water	5	1.14	1.31	1.86
	10	1.35	1.29	2.07
Synthetic wastewater	5	1.91	0.96	2.91
	10	2.62	1.06	3.23

[a] The values are multiplied by 10^{-5} mol L^{-1}.
[b] Concentrations of **T-CSS** were 1, 1.03 and 1.05 $\times 10^{-4}$ mol L^{-1}; and the values of pH were 5.3, 5.5 and 5.7.
[c] %RSD, relative standard deviation.

Table 3

Comparison between proposed measured by T-CSS and reference measured by ICP-OES for determination of UO_2^{2+} in aqueous real samples.

Sample	Proposed measured (n = 3)				Reference measured (n = 3)	
	UO_2^{2+} Average measured [a] ± CL [a,b]	%RSD [c]	*t*-test [d]	*F*-test [d]	UO_2^{2+} Average measured [a] ± CL [a,b]	% RSD [c]
M1	6.30 ± 0.74	4.76	0.48	2.25	6.20 ± 0.49	3.22
M2	7.40 ± 0.66	3.57	0.75	3.00	7.27 ± 0.38	2.10
M3	8.67 ± 0.63	2.90	0.94	2.11	8.50 ± 0.43	2.03
M4	9.80 ± 0.43	1.76	3.60	2.25	9.37 ± 0.29	1.23
M5	10.8 ± 0.79	2.98	1.13	4.43	10.5 ± 0.38	1.45
M6	12.5 ± 1.14	3.66	0.65	3.00	12.3 ± 0.66	2.15

[a] The values are multiplied by 10^{-5} mol L^{-1} for measured.
[b] CL, confidence limits were calculated from: CL =±tS/(n)½. The tabulated value of t is 4.303, at the 95% confidence level; S = standard deviation and n = number of measurements.
[c] %RSD, relative standard deviation.
[d] Theoretical values of *t*- and *F*-tests at 95% confidence limits are 4.303 and 19.0, respectively.